

Diagnostic performance of the quantification of myocardium at risk from MPI SPECT/CTA 2G fusion for detecting obstructive coronary disease: A multicenter trial

Marina Piccinelli, PhD,^a Cesar Santana, MD,^a Gopi Kiran R. Sirineni, MD,^b Russell D. Folks, CNMT, RT(N),^a C. David Cooke, MSEE,^a Chesnal D. Arepalli, MD,^a Santiago Aguade-Bruix, MD,^c Zohar Keidar, MD,^d Alex Frenkel, MD,^d Ora Israel, MD,^d Jaume Candell-Riera, MD,^c and Ernest V. Garcia, PhD^a

^a Department of Radiology and Imaging Sciences, Emory University School of Medicine, Atlanta, GA

^b CHI Health-Creighton University Medical Center, Omaha, NE

^c Vall d'Hebron University Hospital, Barcelona, Spain

^d Rambam Health Care Campus, Haifa, Israel

Received Aug 21, 2016; accepted Dec 5, 2016

doi:10.1007/s12350-017-0819-x

Background. The effective non-invasive identification of coronary artery disease (CAD) and its proper referral for invasive treatment are still unresolved issues. We evaluated our quantification of myocardium at risk (MAR) from our second generation 3D MPI/CTA fusion framework for the detection and localization of obstructive coronary disease.

Methods. Studies from 48 patients who had rest/stress MPI, CTA, and ICA were analyzed from 3 different institutions. From the CTA, a 3D biventricular surface of the myocardium with superimposed coronaries was extracted and fused to the perfusion distribution. Significant lesions were identified from CTA readings and positioned on the fused display. Three estimates of MAR were computed on the 3D LV surface on the basis of the MPI alone (MAR^P), the CTA alone (MAR^A), and the fused information (MAR^F). The extents of areas at risk were used to generate ROC curves using ICA anatomical findings as reference standard.

Results. Areas under the ROC curve (AUC) for CAD detection using MAR^F was 0.88 (CI = 0.75-0.95) and for MAR^P and MAR^A were, respectively 0.82 (CI = 0.69-0.92) and 0.75 (CI = 0.60-0.86) using the $\geq 70\%$ stenosis criterion. AUCs for CAD localization (all vessels) using MAR^F showed significantly higher performance than either MAR^A or MAR^P or both.

Conclusions. Using ICA as the reference standard, MAR as the quantitative parameter, and AUC to measure diagnostic performance, MPI-CTA fusion imaging provided incremental diagnostic information compared to MPI or CTA alone for the diagnosis and localization of CAD. (J Nucl Cardiol 2018;25:1376–86.)

Key Words: Multimodality image fusion • coronary artery disease • image quantification

Electronic supplementary material The online version of this article (doi:10.1007/s12350-017-0819-x) contains supplementary material, which is available to authorized users.

The authors of this article have provided a PowerPoint file, available for download at SpringerLink, which summarises the contents of the paper and is free for re-use at meetings and presentations. Search for the article DOI on www.SpringerLink.com.

Reprint requests: Marina Piccinelli, PhD, Department of Radiology and Imaging Sciences, Emory University School of Medicine, 1364 Clifton Rd, NE, Atlanta, GA, 30322; mpiccin@emory.edu

All editorial decisions for this article, including selection of reviewers and the final decision, were made by guest editor Andrew J. Einstein, MD, PhD, Associate Professor of Medicine (in Radiology), Columbia University.

1071-3581/\$34.00

Copyright © 2017 American Society of Nuclear Cardiology.

Abbreviations

1G	First generation
2G	Second generation
MAR	Myocardium at risk index
MAR ^P	Physiological MAR
MAR ^a	Anatomical MAR
MAR ^f	Fused myocardium at risk
MPR	Multi-planar reformatting
DS	Degree of stenosis
MIP	Maximum intensity projections
AUC	Area under the ROC curve

See related editorial, pp. 1387–1389

INTRODUCTION

Research in the field of coronary artery disease (CAD) management has highlighted the importance of evaluating both anatomy and physiology to provide the appropriate treatment.^{1,2} These considerations have prompted the development of *3D multimodality image fusion approaches* to integrate the complementary information provided by the two modalities and help prevent unnecessary procedures.³

Previously, we evaluated the diagnostic performance of our first generation (1G) 3D MPI-CTA image fusion^{4,7} where we warped the coronaries extracted from the CTA onto the 3D myocardial perfusion distribution. The evaluation was done via visual assessment of the two diagnostic modalities, separated and fused. The aim of the present work is to present the multicenter validation of our second generation (2G) 3D MPI-CTA image fusion algorithm for the quantitative assessment of CAD. The perfusion distribution is mapped onto a CTA-derived biventricular model of the heart with superimposed coronary trees.⁸ The *myocardium at risk index (MAR)* is also automatically estimated by means of our fusion approach. The concept of MAR was introduced decades ago to relate the anatomic size of a coronary bed, i.e., the amount of myocardial mass supplied by a given artery, to the size of an ischemic area determined by an occlusion along that artery,^{9,10} all measures with crucial prognostic value. In the current study, coronary lesions are interactively positioned on the fused display to quantitatively extract a *fused MAR* as results of both anatomical and functional measurements, i.e., from CTA and MPI, respectively. Anatomical findings from invasive coronary angiography (ICA) were used here as the reference standard to validate the diagnostic performance of our method for diagnosing obstructive coronary disease.

MATERIALS AND METHODS

Study Population

Fifty-three patients were initially enrolled and consented at the three centers participating in the study: Emory

University Hospital in Atlanta, USA; Vall d’Hebron University Hospital in Barcelona, Spain; and Rambam Health Care Campus in Haifa, Israel. The study was approved at each institution by the local internal review board and written informed consent was obtained from each patient in accordance with their guidelines on human investigations. Fifteen patients were enrolled at Emory Hospital, 20 at Vall d’Hebron Hospital, and 18 at Rambam Hospital. All the patients underwent stress/rest SPECT MPI, CTA and were afterwards scheduled for a catheterization procedure. The three procedures were performed within a window of 90 days without intervening relevant therapeutic or clinical changes reported. Five patients (2 Emory, 2 Vall d’Hebron, and 1 Rambam) were successively excluded due to issues during the different steps of processing/reading: in two cases the CTA quality was not deemed sufficient to perform a clinical evaluation; three cases were excluded because the automated registration procedure did not properly converge, providing obvious unreliable results. Forty-eight patients—average age 61 ± 9 years; 39 males (81%)—were eventually analyzed in the present study. Table 1 summarizes our patients’ demographics and CAD risks prevalence.

SPECT Myocardial Perfusion Imaging and Protocol

All patients underwent SPECT MPI, exercise stress/rest Tc-99m Tetrofosmin or Sestamibi using either a dual head Millennium MG Camera (GE Healthcare, USA) or a dual head Siemens E-CAM (Erlangen, Germany). These cameras were equipped with Gd-153 sources for attenuation correction (AC).

Standard rest and stress image acquisition protocols were used, detailed information can be found elsewhere.⁴ The Tc-99m doses were adjusted for body weight and ranged 9-15 mCi for rest and 22-45 mCi for stress.

Table 1. Clinical and demographic characteristics of 48 enrolled subjects

Enrolled Patients (Emory–Vall d’Hebron–Rambam) n = 48	
Mean age	61 ± 9 years
Male	39 (81%)
Race	
African American	5
Caucasian	42
Hispanic	0
Asian	1
Unknown	0
Hypertension	34 (64%)
Diabetes mellitus	9 (17%)
Hyperlipidemia	29 (55%)
Smoking	17 (32%)
Prior myocardial infarction	14 (26%)
Prior revascularization	9 (17%)

Computed Tomographic Coronary Angiography and Protocol

Coronary CTAs were performed with a GE LightSpeed VCT 64-slice (GE Healthcare) at Rambam Center, a Siemens Sensation 64-slice (Erlangen, Germany) CT scanner at Emory, and a Philips Brilliance 64-slices at Vall d'Hebron Hospital.

Clinical protocols for a coronary angiography exam were similar between the three institutions and could be briefly summarized as follows. Once the scan delay time was defined, a bolus of 100-120 cc of iodinated contrast of Omnipaque 350 was injected at a rate of 5 cc/sec followed by a saline bolus of 30 cc to flush the contrast agent at a rate of 5 cc/sec. Scan acquisition was initiated after delay time with standard routine parameters (120 KVP, 600-800 effective mAs, pitch 0.2 with helical acquisition, $64 \times 0.6 \text{ mm}^2$ detector configuration). In case of irregular heart rate, β -blocker was given prior to acquisition to keep the optimal range of 60-65 bpm. Images were reconstructed using retrospective ECG gating at a phase of the R-R interval to allow a relative motion-free visualization of the three main coronary arteries. This phase usually ranged between 50 and 70% of the cycle. Transaxial views were used for the subsequent image processing operations. Pixel planar resolutions ranged (0.37-0.49) mm with a slice thickness of (0.62-0.75) mm for scans acquired at Emory Hospital; (0.49-0.61) mm with a slice thickness of 0.62 mm for the acquisitions at Rambam; and (0.357-0.54) mm with a slice thickness of (0.625-0.90) mm for those at Vall d'Hebron.

Invasive Coronary Angiography

Coronary angiography was performed following standard percutaneous techniques on all enrolled patients. Two experienced angiographers examined all invasive studies visually assessing the severity of the stenosis and reported the results by consensus. The minimum criterion for a clinical significant narrowing and presence of disease was 50% degree of stenosis (DS) in at least one major coronary artery. A threshold of 70% DS was also used to classify disease presence and applied for subsequent statistical analysis. For comparison with perfusion studies, lesions of the left main coronary $>40\%$ were recorded

as additional left anterior descending coronary artery (LAD) and left circumflex (LCX) disease. As for the main side branches, diagonals lesions were considered as LAD disease and obtuse marginal artery stenosis were considered part of the LCX territory. Lesions along the posterior descending branch were recorded in the right coronary artery (RCA) territory.

Image Processing and Analysis

All image datasets were collected in DICOM format for further processing and analysis. For each patient, the following image processing tasks and procedures were performed.

CTA Processing: Myocardium and Coronary Extraction. An in-house developed software was used for the interactive manual delineation of the right (RV) and left ventricle (LV) epicardial and endocardial borders then used to generate binary masks (Fig. 1A and B). The CardIQ program module in Advantage Windows Ver-4.2 (GE Healthcare, USA) was used by a CTA expert (CDA) to detect and reconstruct the main coronary arteries and their visible branches. The coronaries were semi-automatically segmented and the information about their location and radii transferred to the workstation handling the fusion process. Models of the coronary trees could be reconstructed and displayed on top of the CTA-derived myocardium (Fig. 1C).

The CTA scans were then interpreted by a second CTA expert (GKRS) blinded to the ICA findings. Interpretation consisted in locating the lesions on a schematic drawing of the main arteries and side branches (Fig. 2) and visually grading the disease severity (normal, $<50\%$, 50-69%, 70-99%, and 100% DS) and lesions composition (calcified, non-calcified, mixed, or unable to determine). The reader also graded the presence and severity of disease on a 5-point scale (definitely normal, probably normal, equivocal, probably abnormal, and definitely abnormal) for global CAD and per territory (LAD, LCX, and RCA) and the quality of the overall acquisition as excellent, adequate, or suboptimal. Interpretation was performed on the original transaxial CTA DICOM images by means of standard display techniques: multi-planar reformatting (MPR), curved MPR, real-time oblique, and sliding maximum intensity projections.

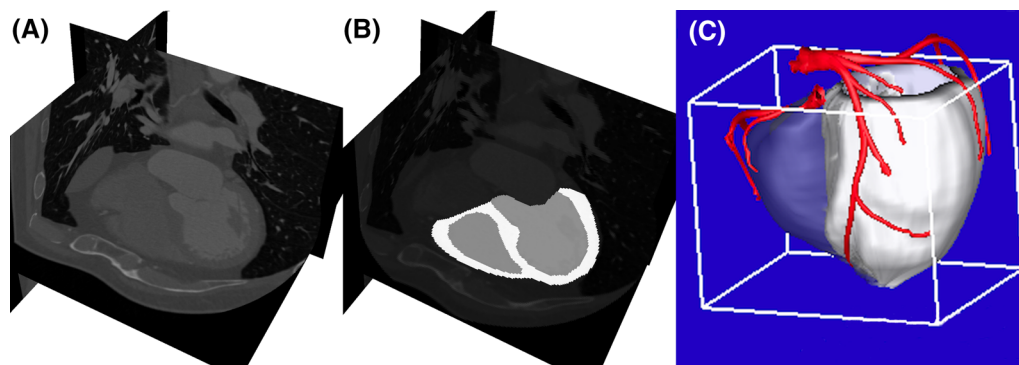


Figure 1. CTA-derived anatomy: (A) original CTA volumetric acquisition; (B) “labeled” CTA with myocardium, left and right chambers classification; (C) 3D biventricular surface representation with superimposed coronary artery.

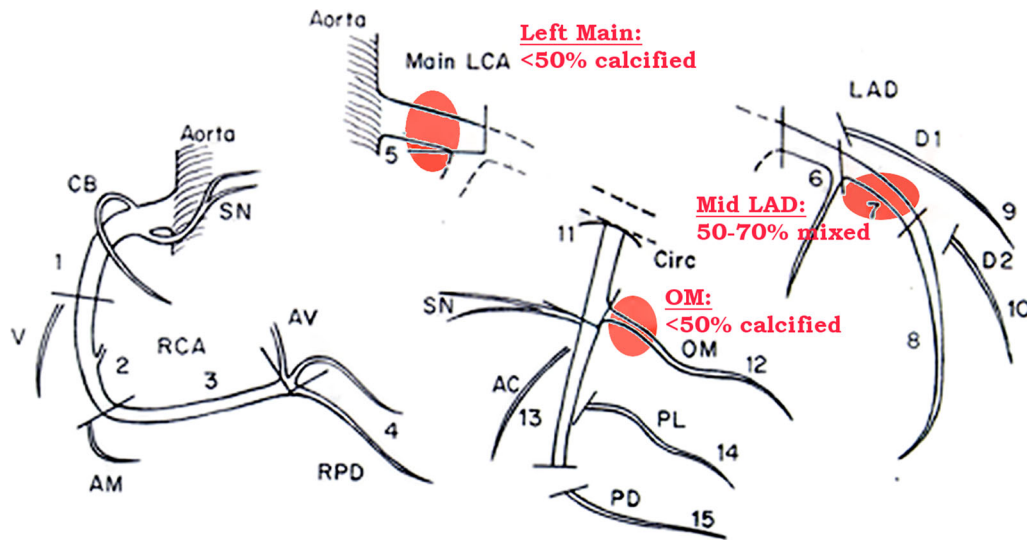


Figure 2. Diagram for CTA reading. Location, degree of stenosis, and composition of atherosclerotic plaques are identified on CTA acquisitions by an expert cardiologist for one of the analyzed cases.

All stenoses evaluated $\geq 50\%$ DS were included in this study. Their locations on the drawings were used to place stenoses on the coronary trees of the 3D display by the operator performing the MAR assessment. For sequential critical lesions, the location of the most proximal significant coronary lesion was used for both for CTA and ICA analysis. Sequential non-critical lesions were not analyzed. For non-sequential critical lesions identified by CTA in the same vessel (e.g., first diagonal + distal LAD), both lesions were used for the MAR^a territory and for potential intersection with the MAR^p territory for the MAR^f determination.

MPI SPECT Processing. ECTb¹¹ was used for the automated processing of nuclear images and fusion procedure. The normal database quantification approach was used to detect hypoperfused areas on the relative stress/rest perfusion maps. The extent of the abnormality was estimated from the 3D perfusion distribution and expressed as a percentage of compromised myocardium per territory and for the total LV (Fig. 3). Since not all patients underwent transmission imaging, MPI quantification was performed for all the available cases without AC and successively redone for the cohort with available AC.

Image Fusion and Quantification of Myocardium at Risk. Two main aspects differentiated our second generation image fusion with respect to our previous ones.⁸ First, the registration follows a voxel-based approach by employing the intensity values of the two volumetric images. Second, both LV and RV are used to obtain the final CTA/SPECT automatic alignment, in contrast to our first generation approach which only used the LV for image fusion leading to lack of constraint in the alignment. Briefly, the registration algorithm consisted of the following image processing tasks. The CTA-derived LV chamber was automatically identified, re-oriented in short axis and rigidly registered to the MPI-derived

LV by maximizing the product of their binary masks over all possible 3D rotations and translations. The transformation obtained was then applied to the full myocardium mask, smoothed with a Gaussian filter and multiplied to the original perfusion image to remove the extra cardiac activity. Finally, *mutual information* was maximized between masked MPI and smoothed CTA with both LV and RV reducing the problems relating to symmetry often encountered when only the LV is used.⁸ A realistic 3D display of the fused images was then created by mapping the MPI-derived measurements, such as relative perfusion or the extent of defects, onto the CTA-derived biventricular model of the heart. Since MPI data are not commonly quantified for the RV, it was represented with a transparent surface and only used during the fusion process. Being reconstructed from the same CTA scan, coronaries could directly be superimposed to the heart model and the 3D perfusion data without warping or the modification of the reconstructed coronary models, a necessary step in our previous approaches.

Quantification of the MAR^{9,10} was then performed based on the MPI data alone, the CTA readings, and on the fused display. These different estimates of the location and extent of myocardial impairment were computed on the 3D LV surface and provided as percentages of the total LV. *The physiological MAR (MAR^p)* was defined as the areas of hypoperfused myocardium according to quantitative MPI, i.e., the black-out maps (Figs. 3B and 4A). Conventional quantitative criteria for ECTb ($\geq 3\%$ LV/ $\geq 10\%$ regional) were used to detect ($\geq 3\%$ LV) and localize ($\geq 10\%$ vascular territory) CAD to a vascular territory. By means of an interactive display and on the basis of the CTA readings provided by means of the schematic drawings of Fig. 2, lesions were placed on the coronary models, and the myocardium subtended to the diseased artery path downstream the lesion location could be computed (Fig. 4B). The definition of the myocardium subtended a

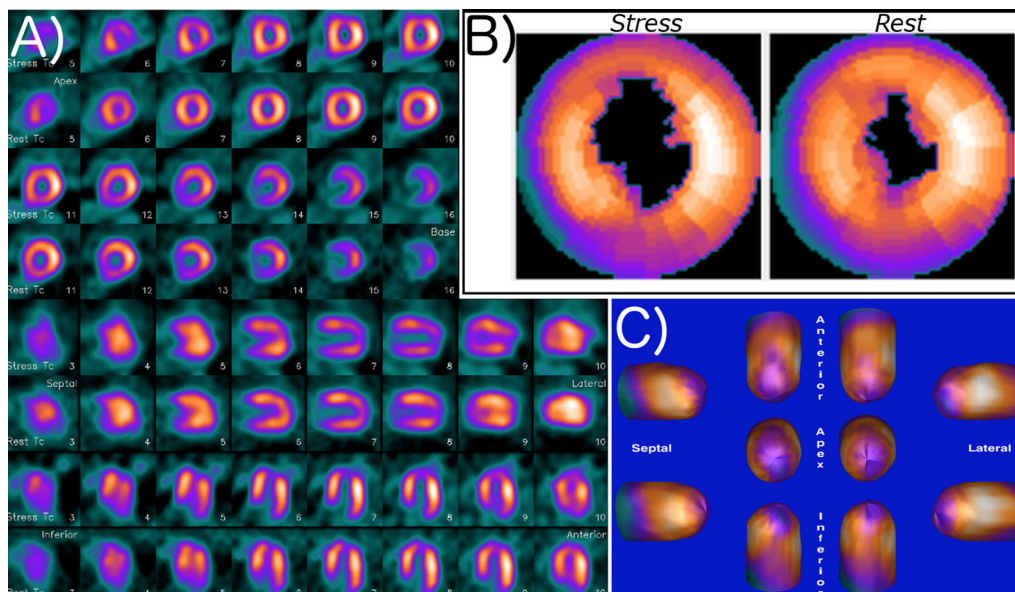


Figure 3. MPI quantification by means of different modules within the Emory Cardiac Toolbox for one of the analyzed cases. (A) MPI slices; (B) myocardial perfusion defect extent quantification; (C) 3D rendering of LV perfusion at rest and stress.

specific coronary artery was based on the work of Seiler et al.¹² and identified as the points on the LV surface closer to that specific artery than to any other. This estimate of compromised myocardium, defined as *the anatomical MAR* (MAR^a), was based only on the CTA anatomical findings. Finally, *the fused myocardium at risk* (MAR^f) resulted from the computation of the intersection of the regions used to measure the previous two indexes, the MAR^p and MAR^a (Fig. 4C), as the areas on which both modalities agree on identifying defects. On a per patient basis analysis, all the lesions identified as significant on the CTA readings were included in the fused display and the three indices were recorded (Fig. 4D). The quantitative criteria used to detect and localize CAD for MAR^f were both 1% of the LV and 1% of the vascular territory, respectively.

Statistical Analysis

Continuous data were expressed as mean \pm SD, while discrete variables were expressed as frequency distributions. Area under the curve (AUC) from ROC analysis was used to determine the incremental value of the MAR index obtained from the fused display with respect to the use of MPI alone or CTA alone. A comparison of the three ROC curves was performed by means of a non-parametric approach.¹³ Statistical significance was defined as $P < 0.05$.

On the basis of CTA, patients and lesions with a classification higher than 1 (i.e., definitely normal) were considered, respectively, as diseased subjects and significant lesions to be included in the fused display for the MAR calculation.

ROC analysis was performed to investigate the diagnostic power of the different MAR indices on a per patient basis. The classifications were also used to appraise the indices on the

separate LAD, LCX, and RCA territories. The MedCalc software (V 15.6) was used to perform the statistical analyses.

Anatomical findings reported during ICA were used as the reference standard to assess our measurements diagnostic accuracy. All statistical analyses were run for both ≥ 50 and $\geq 70\%$ DS criteria.

RESULTS

Patients Population and Imaging Quality

Of the 53 patients recruited for this study 5 (3M, 2F) were excluded for technical issues during processing (3 due to failure of the automatic fusion algorithm and 2 due to technically inadequate CTA). The clinical characteristics of the remaining 48 (39 M) evaluable patients enrolled in the study are presented in Table 1. All patients underwent ICA and had high prevalence of risk factors for CAD. The following clinical results are directly provided for the analyzed 48 patients. At ICA, no disease was detected in 4 patients, and additional 4 cases only had non-critical lesions ($< 50\%$ DS). The remaining 40 patients had at least one lesion with $\geq 50\%$ DS and 38 exhibited lesions with $\geq 70\%$ DS. When stratified by the number of vessels and lesion severity, at 50% DS patients with 1-, 2-, and 3-vessel disease were, respectively 14, 11, and 15; at 70% DS patients with 1-, 2-, and 3-vessel disease were, respectively 13, 16, and 9. Lesions $\geq 50\%$ DS were distributed for the main coronary trees as follows: 30 LAD, 28 LCX, and 23 RCA; for $\geq 70\%$ DS there were, respectively, 27 LAD,

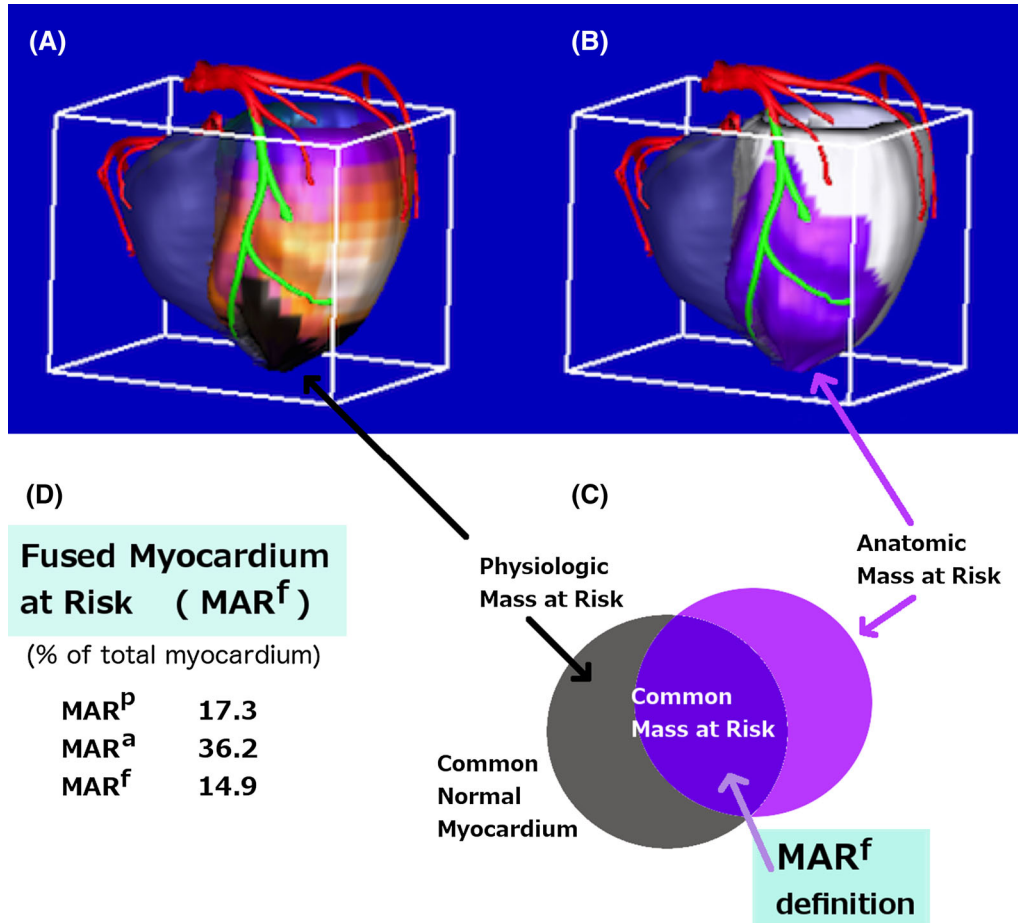


Figure 4. Three approaches for quantification of the percentage of myocardium at risk: (A) according to MPI-derived black-out maps (black area); (B) according to myocardium subtended to a given vessel downstream a CTA lesion (purple area); (C) as the myocardium intersecting the previous two areas (black and purple); (D) Measurement of the three indices: the physiological myocardium at risk (MAR^P), quantitative MPI hypoperfusion; the anatomical MAR (MAR^a) myocardial area distal to the coronary artery stenosis position and subtended to the artery path; the fused MAR (MAR^f), the area of overlap between physiological and anatomical areas at risk.

26 LCX, and 17 RCA. Left main (LM) disease was also reported: 2 cases exhibited lesions with 50% DS; 4 cases 30% DS; and 2 cases lesions with <30% DS.

CTA Image Interpretation

The quality of the CTA images was rated in 10 cases as excellent, 35 adequate, and 3 suboptimal. The reasons for suboptimal studies were the presence of extensive calcifications that prevented a proper visual analysis of the vessels, and coronaries motion, particularly in the RCA territory. When the 48 CTA studies were interpreted 46 patients were classified as abnormal and 2 as normal. Categorized by vascular territories, there were 44 cases LAD, 39 LCX, 37 RCA, and 80 side branches (diagonals, obtuse marginals). Thus between major vessels and side branches a total of 200 lesions

were identified by the CTA expert: 89 presented a 50% DS, 41 between 51-69% DS; 48 between 70-99% and 22 total occlusions.

These classifications on patients and vessel basis were used for the subsequent ROC analysis of the MAR^a using ICA anatomical finding as reference standard.

Myocardial Perfusion Quantification

Conventional database quantification⁷ of the non-attenuation corrected MPI studies (n = 48) identified as abnormal 40 cases and normal 8 cases. Categorized by vascular territories, disease was found in the LAD territory in 20 patients, 17 in the LCX and 18 in the RCA. When the cohort with available AC was considered (n = 38), 33 patients were identified as abnormal; the distribution in vascular territories was as follows: 21

LAD, 14 LCX, and 7 RCA. The AUC under the perfusion ROC curves was determined using the MAR^P calculations with ICA anatomical findings as the reference standard.

Performance of Image Fusion

For all enrolled patients the myocardium was extracted, coronaries reconstructed, and image fusion performed. The anatomy extraction, for both the myocardium and the coronaries, relied on semi-automated methods and was the most time-consuming step of the entire procedure. About 20 minutes on average were needed for the manual definition of epicardial and endocardial CTA borders. The extraction of the coronaries required approximately 7 minutes but increased to as much as 25 minutes for cases with advanced disease and image artifacts. The automatic fusion procedure took no longer than 2 minutes. The accuracy of the final image alignment was visually evaluated for all the cases. Only 38 of these patients underwent transmission imaging and thus were attenuation corrected. Fusion procedure was redone for this cohort with the corresponding MPI quantification.

Performance of MAR^a , MAR^P , MAR^f in Assessing CAD

Once MPI maps and CTA anatomy were aligned, the fusion results were saved and could be opened in successive sessions for the positioning of the CTA-detected lesions and the computation of the two indices, MAR^a and MAR^f . For each case, all significant lesions (>50%) were located by a trained nuclear cardiology expert (CS) on the 3D display according to schematic CTA diagrams and according to the CTA classification. Table 2 lists the global CAD results of the ROC analysis in terms of AUC, 95% confidence interval (CI), and standard error (SE). The analyses were performed by considering all the cases available with the non-AC MPI quantification ($n = 48$) and for the subgroup with available AC ($n = 38$). As a mean of comparison, the analyses were performed also for the smaller cohort with the non-AC MPI quantification. Figure 5 graphically shows the results of the ROC analysis in terms of AUC for the MAR^a (CTA), MAR^P (MPI), and MAR^f (fusion) for localization of CAD by including all vessels in the analysis. In Fig. 5, the AUC plots are displayed for >70% DS without AC, i.e., considering all 48 patients, as a global detection of CAD and specifically for localization on the three territories.

Global CAD Detection. Both Table 2 and Fig. 5 show for all 3 patient subsets, with or without AC. MAR^f showed a trend of better performance in detecting global CAD as compared to MPI and CTA

used alone. These results held for coronary disease defined as $\geq 50\%$ of luminal narrowing as well as $\geq 70\%$ with a slight improvement in performance for the latter. Using the $\geq 70\%$ DS criterion, the non-AC 38 patient cohort showed a close to significant improvement ($P = 0.06$) in MAR^f (AUC = 0.92) as compared to MAR^a (AUC = 0.64).

Global Specificity. Using the $\geq 70\%$ DS criterion, 10 out of the 48 total cases were determined by ICA to have no significant disease. Non-AC MPI correctly identified six of the ten as normal. According to the CTA classification, only 2/10 were identified as normal. When the fused results were considered, there were 8/10 determined as normal.

In the subset of 38 studies for which AC was available, 7 patients were determined to be normal by ICA. Four of these seven cases were correctly identified as normal by MPI; 5 cases were correctly identified as normal by means of the fused approach.

Regional CAD Localization. Figure 5 shows a trend for improved performance of MAR^f over both MAR^a and MAR^P for localization of CAD to the LAD and LCX vascular territories but not for the RCA where MAR^a showed a trend towards better performance. No other significant differences were obtained between any of the MARs when comparing individual territories. Table 3 shows the statistical analysis repeated by combining all three major vessels, 144 for the entire 48 patient set, and 114 for the two 38 patient cohorts. Table 3 shows that when considering for CAD $\geq 50\%$ DS, MAR^f showed a *significantly* higher performance than MAR^P for the all three groups of patients. For CAD $\geq 70\%$ DS, MAR^f showed a trend of improved performance over both MAR^P (with $P < 0.05$) and MAR^a .

DISCUSSION

The present multicenter study shows that our totally automatic quantitative 2G fusion of MPI and CTA shows promise to provide incremental diagnostic value for detection and localization of CAD over either MPI or CTA alone even when using only anatomical ICA findings as a reference standard. Importantly, these results were obtained using totally objective quantitative analysis of the anatomic, physiologic, and fused myocardial mass at risk (MAR) indexes. These MARs were objectively compared using the areas under each ROC curve (AUC) as an indicator of the diagnostic performance of both SPECT non-AC and AC MPI studies either fused or stand-alone and for also CTA. The only subjective component to the study was the visual detection and localization of coronary lesions from the CTA study, consistent with clinical practice and not a part of our image processing development.

Table 2. Detection of global CAD for 50% and 70% DS thresholds

	AUC	95% CI	SE
50% CAD			
Non-AC n = 48 (40,8)			
MAR-fused	0.83	0.965-0.924	0.08
MAR-physiol	0.76	0.611-0.868	0.09
MAR-anat	0.75	0.604-0.864	0.13
Non-AC n = 38 (33, 5)			
MAR-fused	0.87	0.721-0.957	0.07
MAR-physiol	0.80	0.642-0.914	0.07
MAR-anat	0.61	0.429-0.755	0.19
AC n = 38 (33, 5)			
MAR-fused	0.70	0.533-0.840	0.16
MAR-physiol	0.64	0.465-0.786	0.15
MAR-anat	0.61	0.435-0.760	0.18
70% CAD			
Non-AC n = 48 (38, 10)			
MAR-fused	0.88	0.749-0.954	0.07
MAR-physiol	0.82	0.687-0.918	0.08
MAR-anat	0.75	0.601-0.862	0.11
Non-AC n = 38 (31, 7)			
MAR-fused	0.92	0.781-0.982	0.05
MAR-physiol	0.88	0.734-0.963	0.06
MAR-anat	0.64	0.464-0.786	0.14
AC n = 38 (31, 7)			
MAR-fused	0.76	0.595-0.884	0.12
MAR-physiol	0.72	0.552-0.854	0.12
MAR-anat	0.64	0.469-0.789	0.14

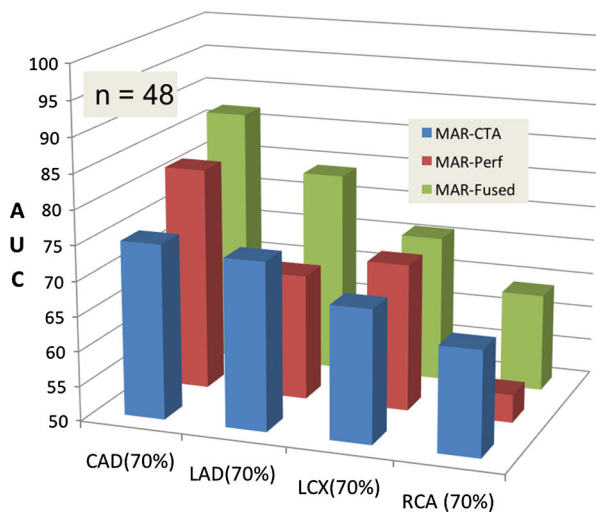


Figure 5. CAD detection and localization results. ROC analysis in terms of area under the curve (AUC) for the MAR^a (CTA), MAR^p (MPI), and MAR^f (fusion) for both detection and localization of CAD with >70% DS.

Previously our team demonstrated⁴ that using our 1G image fusion of MPI and CTA provided incremental diagnostic value over MPI alone or MPI-CTA side-by-side for the detection of obstructive CAD. A marked difference between our previous study and the present one is that in the previous one the MAR concept was not used and the reported results were obtained from the visual analysis of experts of fused, MPI and CTA information. In the present implementation, our MAR^f index is computed as the *intersection* between the anatomical area at risk and the physiological one. The focus of the current study was in fact to diagnose epicardial disease and to design a reliable and objective method to identify with high specificity lesions that would need revascularization. Interestingly, the *union* of anatomical and functional areas at risk could also carry diagnostic information, but it would likely include not only significant epicardial CAD. Although in principle it would be expected that the anatomic mass at risk or even stenosis from CTA should be more related to the

Table 3. Detection of CAD (all vessels included) for 50% and 70% DS thresholds

	<i>AUC</i>	<i>95% CI</i>	<i>SE</i>
50% CAD (pool of all vessels)			
Non-AC n = 144 (79,65)			
<i>MAR-fused</i>	0.71*	0.626-0.780	0.04
<i>MAR-physiol</i>	0.6*	0.513-0.679	0.05
<i>MAR-anat</i>	0.66	0.577-0.737	0.05
Non-AC n = 114 (62,52)			
<i>MAR-fused</i>	0.68*	0.587-0.765	0.05
<i>MAR-physiol</i>	0.57*	0.469-0.658	0.05
<i>MAR-anat</i>	0.66	0.565-0.745	0.05
AC n = 114 (62,52)			
<i>MAR-fused</i>	0.63*	0.536-0.720	0.05
<i>MAR-physiol</i>	0.51*⁺	0.412-0.602	0.05
<i>MAR-anat</i>	0.66⁺	0.564-0.745	0.05
70% CAD (pool of all vessels)			
Non-AC n = 144 (70,74)			
<i>MAR-fused</i>	0.72	0.635-0.788	0.04
<i>MAR-physiol</i>	0.64	0.559-0.721	0.05
<i>MAR-anat</i>	0.64	0.557-0.720	0.05
Non-AC n = 114 (53,61)			
<i>MAR-fused</i>	0.69	0.600-0.776	0.05
<i>MAR-physiol</i>	0.62	0.525-0.710	0.05
<i>MAR-anat</i>	0.64	0.544-0.727	0.05
AC n = 114 (53,61)			
<i>MAR-fused</i>	0.70*	0.608-0.783	0.05
<i>MAR-physiol</i>	0.60*	0.501-0.688	0.05
<i>MAR-anat</i>	0.64	0.544-0.727	0.05

Test significantly different, with indicated *P* values are given in bold

* *P* < 0.05; ⁺ *P* < 0.05

anatomical ICA findings than the MAR (from SPECT/CTA), our results and that of others¹⁴ show that the combined anatomic + physiologic evaluation yields better accuracy. This may be attributed to technical CTA issues such as trying to evaluate a heavily calcified plaque.

Another difference in the present study was the use of our totally automatic 2G image fusion algorithm which uses the CTA-derived LV and RV endo- and epicardium with the coronary tree inherently fused to the distribution. Additionally, our previous validation population was enriched with patients with low likelihood of CAD, which benefited the improved specificity of the fusion process over the stand-alone modalities, an important reason why AC did not add diagnostic performance in the present study. In this evaluation, ICA was used as the standard for all patients. We previously used a mixture of PET and SPECT studies as well as 16 and 64 slice CT systems; here, all MPI studies used SPECT and CTA scans were all done with 64 slice

systems. On the other hand, the population analyzed in the current study was prevalently composed by male subjects at high risk of CAD.

Others have also performed MPI + CTA image fusion, using either our 1G fusion method¹⁴ or other coregistration algorithms.¹⁵ These single center studies required manual alignment of either the CTA, or MPI studies or both, and the results were obtained using visual interpretation of the stand-alone and fused images. An exception has been the work of Slomka et al¹⁶ who developed a more automatic method of aligning the CTA and MPI volume and using the CTA information to adjust the MPI vascular territories before submitting the study to conventional MPI quantification. Their results showed with the $\geq 70\%$ DS criterion improved AUC for the LCX and RCA vascular territories compared to MPI but not the LAD and none vs. CTA. The concept of MAR was not used for evaluating the stand-alone or fused studies. All of these studies concluded that MPI/CTA fusion added diagnostic

information on the functional relevance of coronary artery stenoses.

There are several limitations to our study. Most importantly was the use of the anatomic ICA information as a reference standard. It has been largely demonstrated that no clear relationship exists between DS, its hemodynamic effects, and the actual presence of ischemia.¹⁷ It has also been shown that FFR-guided revascularization significantly improves outcomes and as a consequence functional measurements are now included in revascularization guidelines.^{18,19} The use of ICA-derived anatomical finding as “ground truth” to validate our study may have an impact on the final results. Another limitation is that our MAR quantification depended on relative perfusion quantification¹¹ and visual detection and localization of the CTA coronary lesions. PET-derived absolute myocardial blood flow and flow reserve has been shown to have incremental clinical value over relative quantification in CAD detection particularly multivessel disease.²⁰ Crucial to the development of our fusion framework is the ability to incorporate whenever available any additional information, functional and/or anatomical. Future directions for our fusion methodology are indeed to include absolute measures of myocardial blood flow and flow reserve obtained from dynamic PET acquisitions.

Another important limitation was the manual definition of the RV and LV endo/epicardium from the CTA studies. For the multimodality image fusion approach to gain clinical relevance, the anatomy segmentation has to be almost automatic. This represents an important topic of our developments. Our approach is based on level set segmentation methodologies and shape priors usage. The complete methodology has been previously validated in an animal model,²¹ while a further validation on the same database of patients employed in this study is undergoing at the moment. Although there are manual steps in the CTA processing, once this processing is completed and the MPI study is processed, these distributions are fused totally automatically and so is the quantification of the fused mass at risk.

A concern in using multimodality image fusion approaches is the potential higher radiation dose to the patient from two radiation procedures instead of one. Recent changes in technologies have mitigated the weight of these considerations especially in view of clinical benefits. New devices such as CZT SPECT cameras, resolution-recovery reconstruction, and stress-only protocols have significantly decreased the radiation dose associated with a clinical MPI study⁷ to <3 mSv.²² Similarly, prospective ECG gating and newer CT scanner detectors can reduce the radiation dose from a CTA study to <1 mSv.²²

NEW KNOWLEDGE GAINED

The clinical significance of our findings is that the diagnostic performance of even a small intersection of anatomical (CTA) and physiological (MPI) LV myocardial regions at risk trends to be better than the diagnostic performance of either modality alone requiring standard larger regions at risk to detect or localize obstructive coronary disease.

CONCLUSIONS

Using ICA as the reference standard, MAR as the quantitative parameter, and AUC as the parameter to measure diagnostic performance, this study demonstrated that MPI-CTA fusion imaging can provide incremental diagnostic information compared to MPI or CTA alone for the diagnosis and localization of CAD.

Acknowledgments

Our colleague Dr. Tracy L. Faber was the originator and leader of this project until her passing on March 24, 2012. This work was supported in part by NIH grant R01-HL-085417 from NHLBI. Dr. Piccinelli's work was funded by a Postdoctoral grant from the AHA SE chapter award number 14POST20150001.

Disclosure

Some of the authors (EVG, RDF, CDC) receive royalties from the sale of the Emory Cardiac Toolbox and have equity positions with Syntermed, Inc. The terms of these arrangements have been reviewed and approved by Emory University in accordance with its conflict of interest policies. The remaining authors do not have any conflicts of interest.

References

1. Blankstein R, Di Carli M. Integration of coronary anatomy and myocardial perfusion imaging. *Nat Rev Cardiol* 2010;7:226-36.
2. Bax JJ, Beanlands RS, Klocke FJ, Knuuti J, Lammertsma AA, Schaeffers MA, et al. Diagnostic and clinical perspective of fusion imaging in cardiology: Is the total greater than the sum of its parts? *Heart* 2007;93:16-22.
3. Piccinelli M, Garcia EV. Multimodality image fusion for diagnosing coronary artery disease. *J Biomech Res* 2013;27:439-551.
4. Santana C, Garcia EV, Faber TL, Sirineni GKR, Esteves FP, Sanyal R, et al. Diagnostic performance of fusion of myocardial perfusion imaging (MPI) and computed tomography coronary angiography. *J Nucl Cardiol* 2009;16:201-11.
5. Peifer JW, Ezquerra NF, Cooke CD, Mullick R, Klein L, Hyche ME, et al. Visualization of multimodality cardiac imagery. *IEEE Trans Biomed Eng* 1990;37:744-56.
6. Faber TL, Cooke CD, Peifer JW, Pettigrew RI, Vansant JP, Leyendecker JR, et al. Three-Dimensional displays of left

- ventricular epicardial surface from standard cardiac SPECT perfusion quantification techniques. *J Nucl Med* 1995;36:697-703.
7. Faber TL, Santana CA, Garcia EV, Candell-Riera J, Folks RD, Peifer JW, et al. Three-dimensional fusion of coronary arteries with myocardial perfusion distributions: Clinical validation. *J Nucl Med* 2004;45:745-53.
 8. Faber TL, Santana CA, Piccinelli M, Nye J, Votaw JR, Garcia EV, et al. Automatic alignment of myocardial perfusion images with contrast-enhanced cardiac computed tomography. *IEEE Trans Nucl Sci* 2011;58:2296-302.
 9. Lowe JE, Reimer KA, Jennings RB. Experimental infarct size as a function of the amount of myocardium at risk. *Am J Pathol* 1978;90:363-80.
 10. Lee JT, Ideker RE, Reimer KA. Myocardial infarct size and location in relation to the coronary vascular bed at risk in man. *Circulation* 1981;64:526-34.
 11. Garcia EV, Faber TL, Cooke CD, Folks RD, Chen J, Santana C. The increasing role of quantification in nuclear cardiology: The Emory approach. *J Nucl Cardiol* 2007;14:420-32.
 12. Seiler C, Kirkeeide RL, Gould KL. Measurement from arteriograms of regional myocardial bed size distal to any point in the coronary vascular tree for the assessing anatomic area at risk. *J Am Coll Cardiol* 1993;21:783-97.
 13. DeLong ER, DeLong DM, Clarke-Patterson DL. Comparing the areas under two or more correlated receiver operating characteristic curves: A non-parametric approach. *Biometrics* 1988;44:837-45.
 14. Rispler S, Keidar Z, Ghersin E, et al. Integrated single-photon emission computed tomography and computed tomography coronary angiography for the assessment of hemodynamically significant coronary artery lesions. *J Am Coll Cardiol* 2007;49:1059-67.
 15. Gaemperli O, Schepis T, Valenta I, et al. Cardiac image fusion from stand-alone SPECT and CT: Clinical experience. *J Nucl Med* 2007;48:696-703.
 16. Slomka PJ, Cheng VY, Dey D, et al. Quantitative analysis of myocardial perfusion SPECT anatomically guided by co-registered 64-slice coronary CT angiography. *J Nucl Med* 2009;50:1621-30.
 17. Gould KL, Lipscomb K, Hamilton GW. Physiologic basis for assessing critical coronary stenosis. *Am J Cardiol* 1974;33:87-94.
 18. Tonino PA, Fearon WF, DeBruyne B, Oldroyd KG, Leeser MA, Ver Lee PN, et al. Angiographic versus functional severity of coronary artery stenoses in the FAME study fractional flow reserve versus angiography in multivessel evaluation. *J Am Coll Cardiol* 2010;55:2816-21.
 19. De Bruyne B, Pijls NH, Kalesan B, Barbato E, Tonino PA, Piroth Z, et al. Fractional flow reserve-guided PCI versus medical therapy in stable coronary disease. *N Engl J Med* 2012;367:991-1001.
 20. Bateman TM, Gould KL, Di Carli MF. Quantitation of myocardial blood flow. *J Nucl Cardiol* 2015;22:571-8.
 21. Piccinelli M, Faber TL, Arepalli CD, Appia V, Vinten-Johansen J, Schmarkey SL, et al. Automatic detection of left and right ventricles from CTA enables efficient alignment of anatomy with perfusion data. *J Nucl Cardiol* 2014;21:96-108.
 22. Einstein AJ, Berman DS, Min JK, et al. Patient-centered imaging: shared decision making for cardiac imaging procedures with exposure to ionizing radiation. *J Am Coll Cardiol* 2014;63:1480-9.